Effects of Willamette Valley Sedimentary Structure on Ground Motions

by

Roey Shimony

A thesis accepted and approved in partial fulfillment of the

requirements for the degree of

Master of Science

in Earth Sciences

Thesis Committee:

Valerie Sahakian, Research Advisor

Emilie Hooft, Chair

Diego Melgar, Member

Josef Dufek, Member

University of Oregon

Fall 2024

THESIS ABSTRACT

Roey Shimony

Master of Science in Earth Sciences

Title: Effects of Willamette Valley Sedimentary Structure on Ground Motions

Accurately estimating ground motions is critical for seismic hazard assessments, particularly in regions like the Cascadia Subduction Zone (CSZ), which has the potential to generate **M**8-9 megathrust earthquakes. This study focuses on the Willamette Valley (WV), an elongated sedimentary structure extending from Eugene to Portland, Oregon, which has been understudied despite being home to most of Oregon's population and infrastructure. The WV is characterized by soft, low-density sediments confined between two mountain ranges, the Oregon Coast Range and the Cascade Range, creating significant lateral contrasts in seismic velocity. Using available geologic, geophysical, and structural data, we constructed new velocity models of the WV basin, varying the basin's depth geometry and seismic velocity structure. To test these models, we performed numerical simulations of three **M**~4 local crustal earthquakes, and compared our synthetic ground motions with recorded data. Our findings indicate that the sedimentary structure of the WV plays a significant role in amplifying ground motions from local earthquakes. This has important implications for seismic hazard assessments in the region, and highlights the need for a detailed representation of the WV's shallow structure in regional seismic velocity models. By refining the understanding of the WV's impact on ground motion, this research contributes to more accurate seismic hazard assessments in the Pacific Northwest, showing the possible regional amplification.

Table of Contents

LIST OF FIGURES

LIST OF TABLES and EQUATIONS

Introduction

Estimating ground motions from future earthquakes is the basis for seismic hazard assessments. Of particular importance are site characteristics, which play an important role in determining the amplitude and duration of shaking, either amplifying or attenuating ground motions at frequencies of engineering interest. The Cascadia Subduction Zone (CSZ) has a relatively high seismic hazard, and is known to produce **M**8-9 megathrust earthquakes with recurrence intervals of ~500 years (Atwater & Hemphill-Haley, 1997; Wirth & Sahakian et al., 2022; Heaton & Hartzell, 1986; Atwater et al., 2016; Kelsey et al., 2005). Recent updates of the US National Seismic Hazard Model (NSHM) (Petersen et al., 2020, 2024) include a focus on the addition of 3D simulation studies to the hazard assessment, using velocity models of sedimentary basins in several regions, including the Pacific Northwest (PNW). In the PNW, recent studies have focused on characterizing the Seattle, Portland, and Tualatin basins due to their ability to amplify earthquake ground motions and increase seismic hazard (e.g., Wirth et al., 2019; Frankel and Grant, 2021). However, the Willamette Valley (WV), extending from Eugene to Portland, is home to most of Oregon's population, major cities, and important infrastructure, yet remains mostly understudied.

Confined by two mountain ranges, the Coast Range to the west and the Cascade Range to the East, the WV is an elongated sedimentary structure filled with relatively soft, low-density material that stands in contrast to adjacent hard rock sites. Most of the WV demonstrates negative values of residual gravity, with the surrounding topographic highs showing positive values (Bassett & Watts, 2015). This implies that the region may be characterized by lower density, slower seismic velocity material mantling higher density,

faster seismic velocity material, which may act seismically as a basin. Although the geologic and seismic velocity structure of the Willamette Valley are not fully constrained, it has been suggested that it may amplify ground motions because of its basin-like sedimentary structure (Silva et al., 1998), as opposed to acting as a more diffuse sedimentary region that attenuates shaking (i.e., the Sacramento-San Joaquin delta, motions (Baltay & Boatwright, 2015; Eberhart-Phillips et al., 2014; Nye et al., 2023). However, no ground motion studies to date have focused on the WV's influence on earthquake ground shaking.

To this end, we construct a new seismic velocity model of the WV basin, using currently available data as constraints. To examine the effect of basin structure on ground motions, we run numerical simulations of local earthquakes using various basin models and compare the synthetic results with observed data from these events. We found that the WV sedimentary structure plays a significant role in amplifying ground motions, as evidenced in observational data from real earthquakes.

Background

The Cascadia Subduction Zone (CSZ) is formed by the oblique convergence of the Juan de Fuca plate beneath the North America plate. The WV is within the Puget-Willamette lowland that includes most of the major cities in Washington and Oregon. This lowland is an active forearc basin, which is presumed to have separated from the offshore basins of the CSZ by the uplift of the Coast Range 15 – 16.5 Ma (McNeill et al., 2000). The Siletz River Volcanics (SRV), part of the large igneous province Siletzia that was accreted to North America (49-51 Ma), are considered the basement rocks throughout the entire WV (Wells et al., 2014). Atop the basement is a thick layer of marine sedimentary

rocks, deposited before the uplift of the Coast Range and the separation of the WV from the oceanic basins. The most recent sediments filling the WV basins are fluvial sediments, a result of the Willamette River alluvial plain.

Although formally a valley, the WV region may exhibit seismic characteristics that are similar to sedimentary basins. Sediments consisting of soft (low density) rocks or soils have long been known to amplify ground motions (Borcherdt & Gibbs, 1976). Enclosed sedimentary basins can further amplify shaking at resonant frequencies during an earthquake as observed in sedimentary basins around the world (Campillo et al., 1989; Wald & Graves, 1998; Cruz-Atienza et al., 2016). Basin-edge effects may also contribute to amplification of ground motions (Kawase, 1996).

Characterizing the effect of such sedimentary structures on shaking can have a significant impact on seismic hazard assessments, and is typically done either observationally with microzonation methods, or with physics-based or empirical modeling. Despite high seismic hazard in the region, the seismically quiet nature of the CSZ makes it difficult to predict shaking intensities based on observational methods. For modeling methods to be accurate, a detailed shallow crustal seismic velocity model is required for both physics-based simulations, as well as empirical ground-motion models (GMMs). Physics-based simulations are strongly dependent on the accuracy of three-dimensional velocity models. GMMs, the industry standard for estimating ground motions in probabilistic seismic hazard analyses (PSHA), still require a velocity model to describe basin effects, utilizing proxies such as Z1.0 and Z2.5 (i.e., the depth to shear wave velocities of 1.0 and 2.5 km/s, respectively).

In the Puget Sound region of Washington State, studies have shown using observational data (e.g., Thompson et al., 2020; Wirth et al., 2018b) and numerical simulations (Frankel et al., 2018; Wirth et al., 2018) that the Puget Lowland and Seattle basin influence the amplitude of ground shaking. These basin structures are included in the USGS Cascadia Velocity Model (USGS CVM, Stephenson et al., 2017a)), the current seismic velocity model used in ground motion simulations for the region. Sediments have been observed in the WV down to 3-4 km overlaying basement rocks (Wang et al., 2019; Ward et al., 2018), but have to date remained relatively understudied, and are not well-constrained in the USGS CVM, as there is limited data to support or describe it. As such, hazard is likely not fully captured in this region.

In this work, we utilize available geologic, geophysical, and structural data for the WV to create a "basin" model for the purpose of earthquake ground motion simulations. Although this region is not a traditional geologic basin, we hereto refer to our structural models and the Willamette Valley as basin models, in line with seismic observations. We validate our model by comparing the synthetic results with recorded data from three local events. This model will serve as an improvement over previous representations of the WV shallow structure, and will improve the ability to assess and understand the effect the WV has on regional grounds motions and seismic hazard.

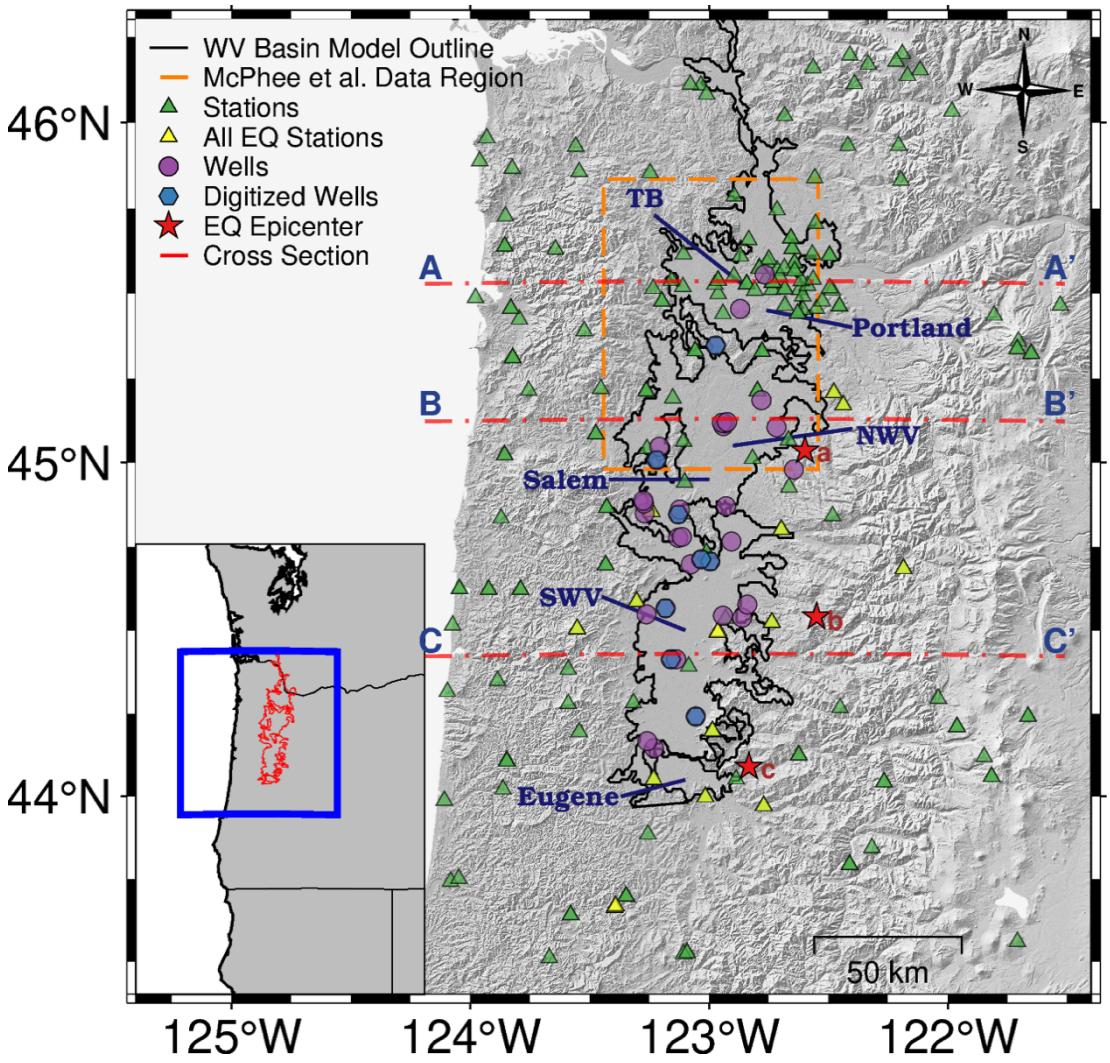

Fig 1. Regional data map of the study area. Solid black line shows the modeled valley outline; Dashed orange line shows the region of the McPhee et al. (2014) data. Green triangles: seismic stations used here; yellow triangles: stations that recorded all three earthquakes modeled; purple circles: oil and gas wells; blue circles: digitized wells that were converted into velocity profiles; red stars: epicentral locations of the three earthquakes modeled (labels are according to Table 1). Dashed red lines indicate locations of basin cross sections shown in Figure 3; TB: Tualatin Basin, NWV: North Willamette Valley, SWV: South Willamette Valley.

Data and Methods

Due to the limited data available to constrain the shallow structure of the WV, we constructed four basin models with varying characteristics (e.g., basin depth geometry and sedimentary seismic velocity structure). We identify the best-fitting model by performing numerical simulations of three local events (Table 1), using both our own models (this study) and the USGS CVM (Stephenson et al., 2017), and comparing the synthetic results with recorded data from these events.

Data

Our models' spatial extent is the same between all four models, and in the absence of structural data, follows the topography of the WV (Figure 1), as defined by the V_{S30} = 400 m/s contour from the USGS terrain-based proxy V_{S30} grid (Yong et al., 2016; Heath et al., 2020). We embed our models into the USGS CVM, so regions outside this domain are identical to the USGS CVM.

In the Portland and Tualatin basins and northern WV, our depth to basement is constrained by from the gravity study of McPhee et al. (2014). In the southern WV, we use interpretations of 36 oil and gas wells from Yeats et al. (1996) for depth to basement constraints (Figure 2), which we define as either the depth to the Eugene-Spencer formation contact or the Siletz River Volcanics (~2.5 km/s and ~3.5 km/s S-wave velocity, respectively). While we cannot constrain the full geometry of the basement with such limited data, these are the most extensive datasets for depth to geological units in the WV and are sufficient for a first order estimate on the depth to basement.

We define seismic velocities in the basin using an average shallow velocity gradient calculated from digitized sonic well log data from 8 wells (Bruer, HJ Miller, Independence,

Ira Baker, Klohs, M&P Farms, Porter Wolerton ; Figure 2c). The sonic logs were in units of units in μs/ft (or slowness), so were first converted to velocity in m/s, and then converted to Vs using the empirical relations from Brocher, (2008). The logs were digitized from scans of the originals, and hence, not all available logs scans were clear enough for this process. The 8 well logs we use in this study are visually the clearest and easiest to digitize with confidence, and with decent spatial coverage throughout the WV. We fit a linear slope to Vs as a function of depth:

$$V_S = a * Z + b \quad (1)$$

where Z is depth in meters and positive down, a = 1.0302, and b = -792.932 m/s . We assign velocities to greater depths by extrapolating this down to the given model's prescribed basement. We recognize that this gradient is likely different, and not linear, within the valley – however as we do not have additional constraints (and as the well constraints are noisy), we take this as our best estimate.

To validate our basin models, we use recorded data from three local **M**~4 crustal earthquakes (Table 1), occurring at different latitudes along the eastern border of the WV. These were the best-recorded events with sufficiently high signal-to-noise ratio to use in validation, and they provide some variable azimuthal coverage. We downloaded recordings from all available seismic stations (broadband and strong-motion) within our domain (Figure 1). For strong-motion instruments, we corrected by the gain and high-pass filtered at 0.28 Hz (i.e., the higher frequency microseism peak). For broadband instruments, we applied an instrument correction and bandpass filter using the tapered frequencies 0.063 Hz, 0.28 Hz, f_N - 5, f_N, where f_N is the Nyquist frequency of the instrument (80 Hz or 100 Hz), and the lowest frequencies represent the most prominent microseism peaks. To

compare with the maximum frequency of our simulations (1 Hz), we additionally low-pass filtered the waveforms with a maximum frequency of 1 Hz with a taper beginning at 0.9 Hz. We also required that recordings have a minimum signal to noise ratio (SNR) of 5. We computed SNR as the ratio of standard deviation of the signal (first 20 seconds after theoretical S-wave arrival using the hypocentral distance and a 3.5 km/s S-wave travel time) and standard deviation of the noise (first 15 seconds before theoretical P-wave arrival the hypocentral distance and a 5.9 km/s P-wave arrival time) as done in Nye et al., (2023).

We categorize stations as 'Valley' or 'Mountain' stations (Table 1, Figure 1), to understand how our models best estimate ground motions where the velocities vary from the USGS CVM. In general, only the Valley stations should vary from USGS CVM, since the velocity structure outside the valley is the same in all models. Though, the Mountain stations can be affected as well by the basin structure in our models.

Label	Name	Event ID	Lon	Lat	Depth (km)	M	Time	Description	Total Recordings	Total Valley recordings
a	Scotts Mills	10563558	-122.5993	45.0353	17.37	3.96	2017-12-14 01:24:2	5 km E of Scotts Mills, Oregon	89	48
b	Salem	11606263	-122.5508	44.5403	13.17	4.2	2022-10-07 12:52:36	58.8 km SSE from Salem, Oregon	106	66
c	Springfield	8477537	-122.8334	44.0896	9.6	4.1	2015-07-04 15:42:18	16 km ENE of Springfield, Oregon	43	13

Table 1. Local earthquakes modeled in this work. Locations are shown in Figure 1.

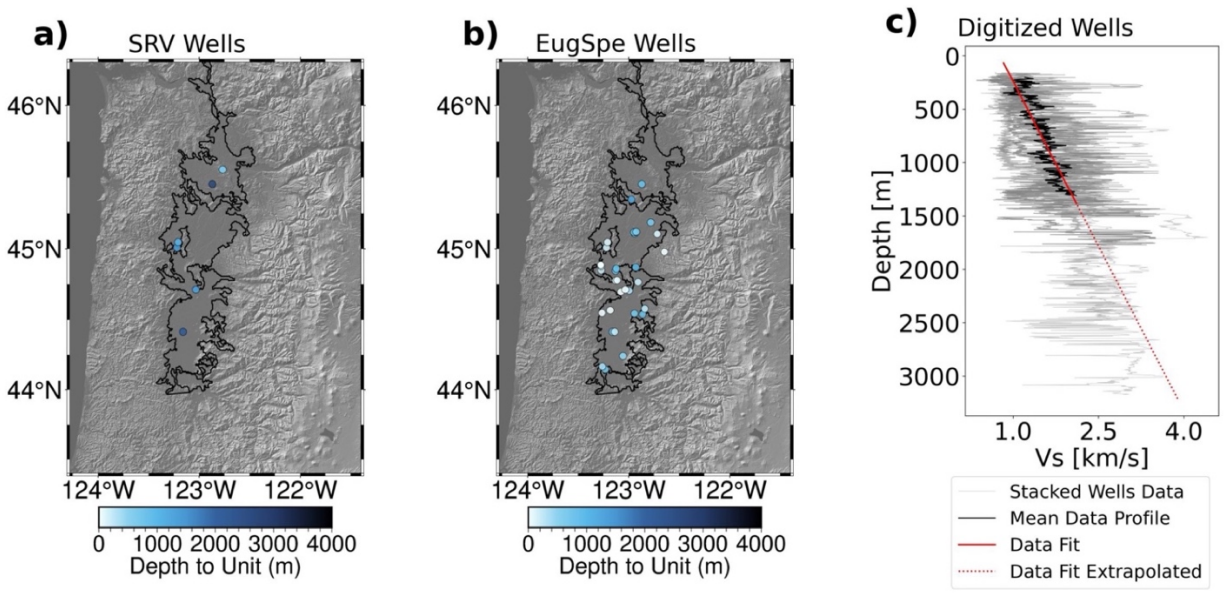

Figure 2. Oil and gas well data. (a) and (b) show the locations of wells used for the WV basin models constructions, colored by depth (bottom colorbar) to wells that recorded depth to the Siletz River Volcanics (SRV) unit and depth to the Eugene/Spencer (EugSpe) formations, respectively. (c) shows digitized well log data converted into velocity profiles. Grey lines: all eight digitized wells stacked together; black line: averaged profile of all digitized wells, calculated up to the depth of the shallowest well; red line: data fit to the averaged profile from Equation 1; dashed red line: is the extrapolated part of the data fit to the deepest well using Equation 1.

Model Construction

Our four models (EugSpe SM, EugSpe 1D, SRV SM, SRV 1D) have two basin geometries: EugSpe and SRV, representing depth to the Eugene-Spencer formation (~2.5 km/s) contact and top of the Siletz River Volcanics (~3.5 km/s), respectively; and two sedimentary filling options (SM: single material, or homogeneous seismic velocity; 1D: one-dimensional velocity gradient as defined in Equation 1). We name models using a description of the "geometry" and "filling", e.g., EugSpe SM has a basement defined by the Eugene-Spencer formation contact with a single-material filling.

We define the basin depth on a regular 2D grid, where each point (longitude, latitude) is assigned a depth (z) value to create a basin depth surface. The spatial extent of the basin is consistent between all models (the V_{S30} = 400 m/s contour line, described above).

To form the basin geometry, we define both depth, and geometric shape. As noted above, we consider two basin bottom constraints. The SRV are considered the true basement rock formation throughout the entire WV. This surface has a maximum depth of ~4000 m. However, we note that seismically, the "basin" bottom may be better represented by an impedance contrast of other units. We consider the Eugene and Spencer formation contact as an impedance contrast representing the top of the harder marine sedimentary (Spencer formation) units and the bottom of the fluvial sedimentary (Eugene formation) units. This surface has a maximum depth of ~2000 m.

For geometric shape, we constrain the northern part of our model (Portland and Tualatin basins and Northern Willamette Valley bounded in the south by ~45 degrees North latitude), based on the depth to basement surface from McPhee et al., (2014), which is interpreted to be the SRV. The middle and southern portions of the Willamette Valley posed greater challenges in defining a two-dimensional basement geometry, due to the lack of constraints. As a proxy, we assume that the basement/basin depth tapers towards the basin edges and is deepest in its center. To construct this, we calculated the distance between each point within the basin to all the points on the basin outlines. We then assigned the minimum value (i.e., the distance from the basin point to the nearest outline point) a depth calibrated (normalized) to fit the basin depth constraints from the oil and gas wells for our two selected geologic surfaces, Eugene-Spencer and SRV formations.

Our two basin "filling" types are a single material filling (V_S = 600 m/s, based on the minimum velocity achievable in the simulations), or a 1D profile. The 1D profile is as described above.

Lastly, we embedded our basin model into the USGS CVM (Stephenson et al., 2017a). We extract a portion of the USGS CVM that fits our domain extent, which spans from latitude 43.4° to 46.7° (~378 km) and longitude -124.2° to -121.5° (~216 km), with a maximum depth of 60 km. Select cross-sections of our four basin models are shown in Figure 3.

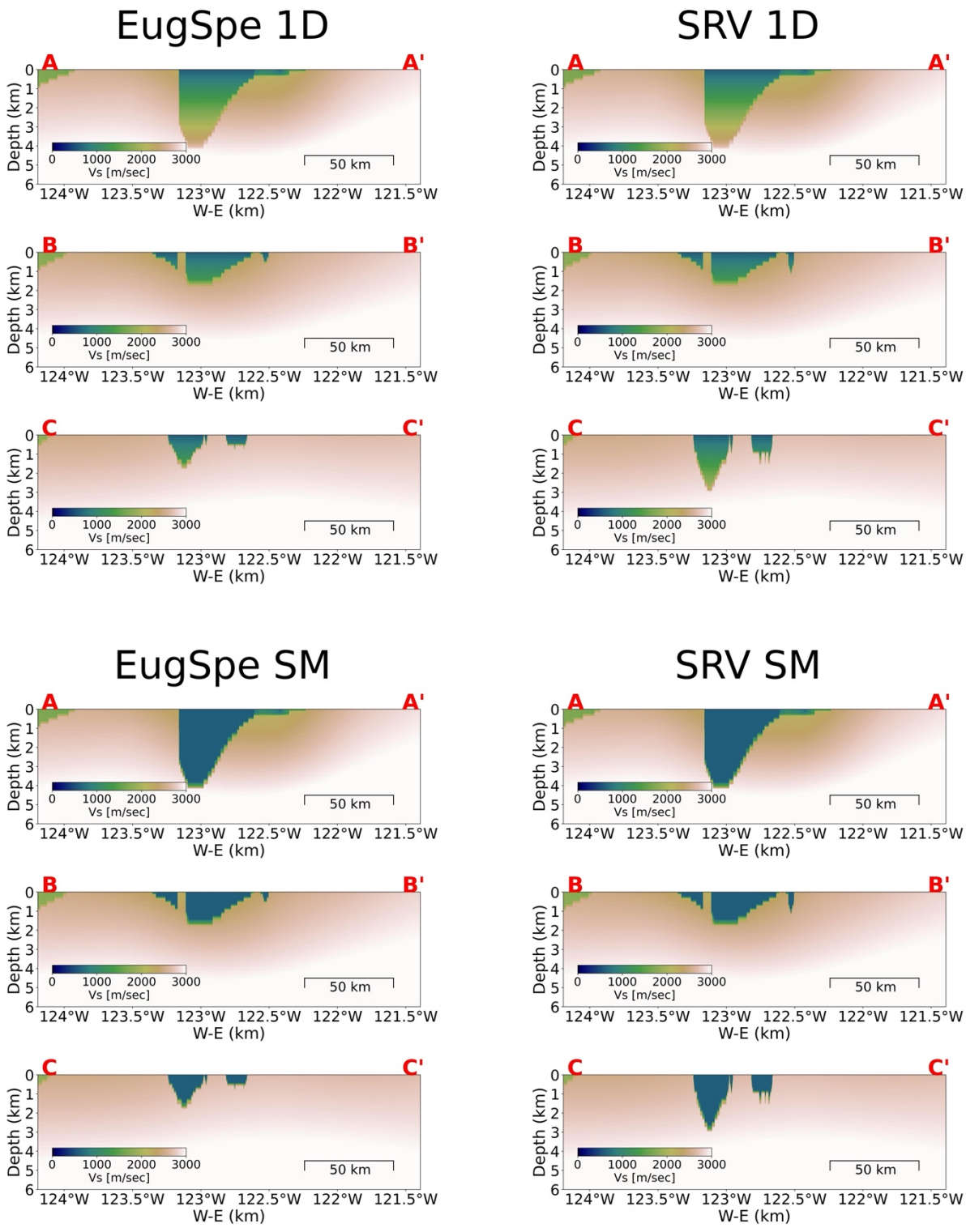

Figure 3. Basin model cross sections (three cross-sections for each of the four models). The locations of the three cross sections are shown in Figure 1.

3D Numerical Simulations

Our 3D synthetic waveforms were computed using SW4 2.01 (Petersson & Sjögreen, 2015, 2017; Sjögreen & Petersson, 2012; Zhang et al., 2021) published under the GPL 2 license. SW4 solves the seismic wave equations in displacement formulation using a 4th order accurate summation-by-parts finite difference method and a 3D velocity model structure. We have converted the velocity model created into an "rfile" format, suitable for SW4 simulations. An "rfile" is a binary structured grid format, and it is the most computationally efficient format for 3D velocity structure in SW4, as well as more effective for smoothly varying 3D heterogenous structure (Petersson & Sjögreen, 2017).

The relationship between the maximum achievable frequency (f_{max}) of the simulations and the domain parameters is described by:

$$f_{max} = \frac{minV_s}{PPW \times h} \quad (2)$$

where $minV_S$ is the minimum shear-wave velocity in the domain, points per wavelength (PPW) describes the number of grid points resolvable within computational stability, and h is the grid point size.

Our parameters were set to achieve the best realistic simulation process, considering simulation and queue time at the University of Oregon High Performance Computer Center, and our model's computational size. The target maximum frequency in this work is 1 Hz, to at a minimum analyze amplification of the longer periods (1 – 10 s) within our computational resources, consistent with other basin ground motion studies in the region (Frankel & Grant, 2021; Thompson et al., 2020; Wirth et al., 2019). We set our minimum V_S value, the velocity value that represent the top of the basin sedimentary

filling, to 600 m/s in most models, with a few final simulations that had minimum V_S of 300 m/s. For the models that have single filling material, we assigned this value throughout the basin. For the 1D velocity gradient models, these values were set as the minimum value of the velocity profile. We set the remainder of the computational parameters based on this f_{max} and minV_S. We use 6 Points Per Wavelength (PPW) in all our simulations. The resultant grid size (h) is 100m for the 600 m/s simulation and 50m for 300 m/s.

A major advantage of SW4 in this work is its ability to set vertical grid size refinement, as our velocity profile increases with depth. The grid sizes mentioned above were selected for waves propagating inside and around the basin. In the remainder of the domain seismic velocities are much higher than in the basins, so we refine our 3D grid twice yielding 3 computational layers: 0 – 4 km, 4 – 10 km and 10 – 60 km, with grid sizes of 100, 200 and 400 m respectively for the minimum V_S = 600m/s models and 50, 100 and 200 for the V_S = 300m/s models.

We simulate our events using a point source that is described using a Gaussian source time function. We set the rise time to 0.25 s, so the source frequency content will be between 0.1 – 10 Hz, consistent with other modeling works in the region that simulated local crustal earthquakes (Thompson et al., 2020; Wirth et al., 2019).

Results

Intensity Measures Residuals

We compare residuals between the observed data and synthetic waveforms from our four models as well as the USGS CVM, for simulations from three local earthquakes (Table 1). We do so for Peak Ground Velocity (PGV), and Fourier Amplitude Spectra (FAS) binned to the frequencies 0.2, 0.3, 0.4, 0.5, 0.6, 0.7 Hz (Bayless & Abrahamson, 2018). We compute residuals as:

$$\delta_{IM} = \ln(IM_{obs}) - \ln(IM_{syn}) \quad (3)$$

where a residual (δ_{IM}) of 0 corresponds to a perfect fit between our synthetic results and the observed. To test how our models perform in the WV against the USGS CVM, we also calculate the ratios between our models' residuals and the USGS CVM residuals:

$$\delta_{RATIO} = \frac{\delta_{IM,CVM}}{\delta_{IM,Model}} \quad (4)$$

where a ratio (δ_{RATIO}) of 1 indicates that there is no difference between our models and the USGS CVM, while ratios over 1 indicates that our basin model provides a better fit to the observational data.

Figure 4 shows a summary of the populations of these residuals for each IM in each model, and earthquake (because the events were recorded on different stations for each earthquake).

The 2022 Salem earthquake (i.e., the most recent event) produced the most recordings in the WV area (66 stations) and hence, the results from this event are the most

statistically robust. Comparisons between our simulation and observations of the Salem earthquake show that our models perform better than the USGS CVM throughout all IMs by approximately 0.5 ln units (Figure 4a), although all four of our basin models perform very similarly. Between IMs the differences in residual values are not very significant. We can notice a slight trend between IMs, where there is an increase in residuals (poorer fit) with increasing frequency. The Scotts Mills earthquake (Figure 4b) show similar trends between models (i.e., our models perform better than USGS CVM), though not as significant as in the Salem Earthquake. Here, there is a slight opposite trend between IMs, where the residual values decrease as frequencies increase. The Springfield earthquake (Figure 4c) has significantly less recordings in Valley stations compared to the other two (13 Valley stations) and is the least statistically valid event. Here, the difference between our models and the USGS CVM is minimal. There is no clear trend in residuals between IMs.

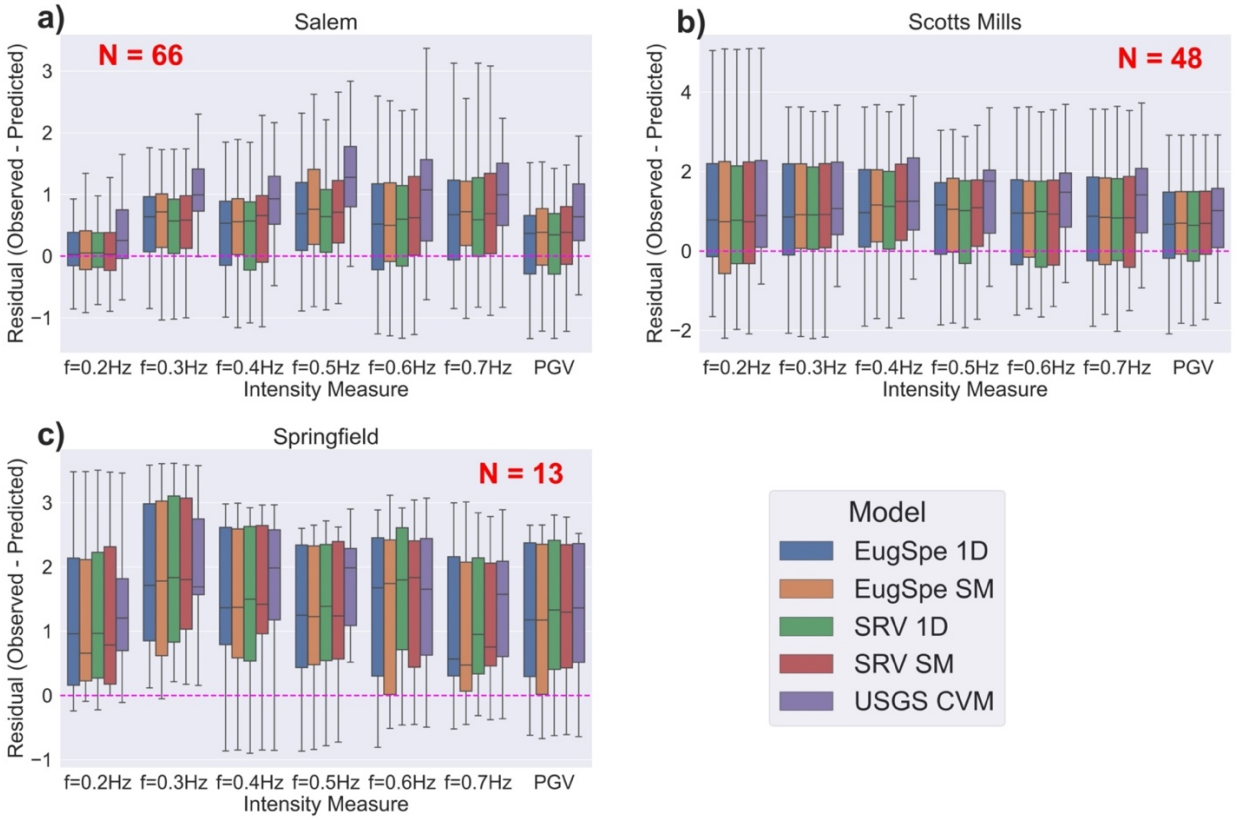

Figure 4. Box and whisker comparison plots of residuals between observed and synthetic waveforms from all models and all earthquakes on Valley stations, for all intensity measures (IMs) residuals calculated (x-axis). (a) Results for the Salem earthquake; (b) Scotts Mills earthquake; (c) Springfield earthquake. Results for each IM are stacked for all models, color indicated by the legend on the bottom right. The number of Valley stations (N) that recorded each earthquake is indicated in bolded red text.

These results show that our models perform better, when compared to observed data, than the USGS CVM in the WV. However, there are not sufficient data (number of recordings, or diverse azimuthal coverage and station coverage) to quantitively describe one of our four models as better than another. Nonetheless, based on regional constraints and geologic interpretations, we expect the SRV_1D model to be the most realistic, as other studies (i.e., McPhee et al., 2014; Wang et al., 2019) suggest the SRV to be the basin

basement at the depths represented in our model, and well logs and structural interpretations suggest there is variability in seismic velocity with depth. Based on this, we select the SRV_1D model as preferred and present further analyses with this model.

We present a spatial representation of PGV ratio residuals between SRV 1D and the USGS CVM (Equation 4) in Figure 5 (additional IMs ratio figures are plotted in Figures S13 – 24), to understand geographic patterns in model performance. Higher ratio values indicate a higher residual for the USGS CVM (i.e., our SRV_1D model performs better), and a ratio value of 1 indicates that our models and the USGS CVM produce the same residual or misfit. Beneath each map we show a corresponding box and whisker plot, showing the distribution of residuals ratio values for Valley and Mountain stations.

For the Salem earthquake, the ratio value distribution is positive for Valley stations and ~1 for the Mountain stations, implying that our model provides an improved fit than the USGS CVM to the Valley stations, but not necessarily the Mountain stations. The Springfield earthquake shows similar results, though, as mentioned before, the number of recordings is significantly lower than the other two earthquakes. This further supports our observation that our basin models perform better than the USGS CVM in the WV.

The results vary for the Scotts Mills earthquake, in which we observe a cluster of stations with ~1 residual ratio in the northern part of the WV. We will further examine this observation in the section on “Inaccuracies of the Basin Model”. We also note that the stations at the southernmost edge of the WV, throughout all earthquakes, show on average a ratio lower than 1 (i.e., the USGS CVM performs better). This implies that this portion of our basin model is less accurate than other regions.

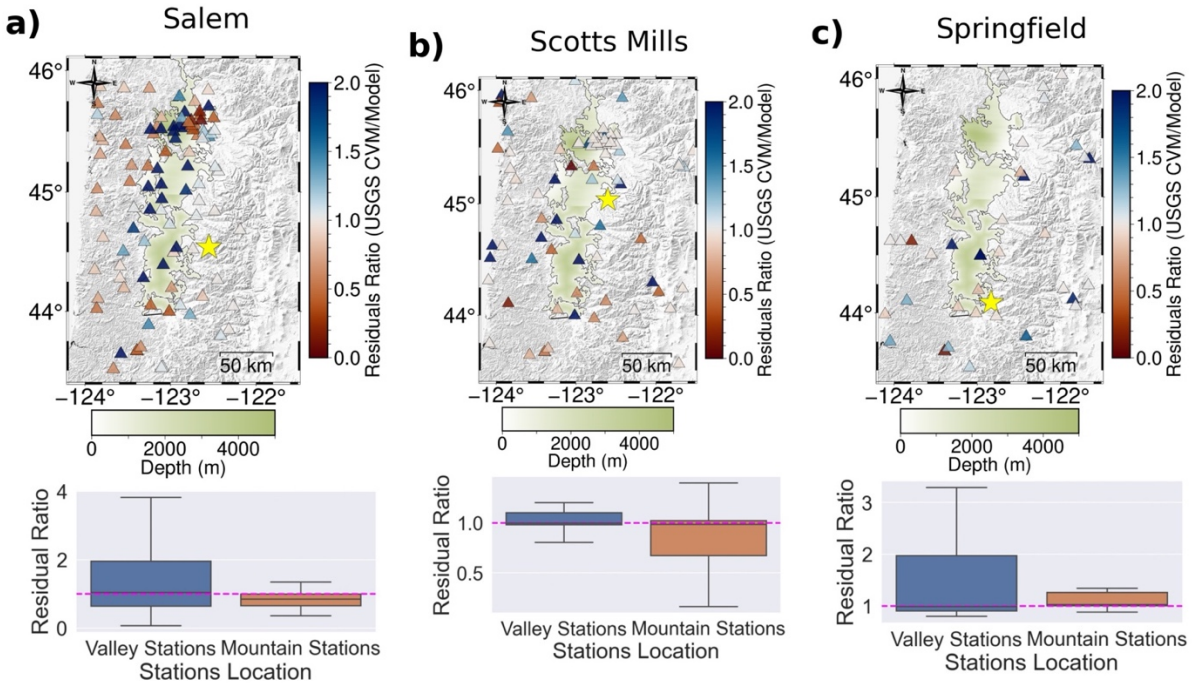

Figure 5. Residuals ratio comparison for the SRV 1D model (Ratio = Stephenson residuals/Model residuals) in map view, and histogram for Valley and Mountain stations . Maps show PGV residual ratios (Equation 4) from the (a) Salem, (b) Scotts Mills and (c) Springfield earthquakes (yellow stars). The panels show all stations (triangles - including mountain stations), colored by residual ratio (colorbar on right). The Willamette Valley is colored by the depth of our SRV 1D WV basin model (preferred model).

We also show absolute IM residuals maps in Figure 6 for f = 0.3, 0.5, 0.7 Hz and PGV (additional intensity measures are plotted in Figures S1 - 12), separating the WV into three regions for our discussion here: 1) Southern, latitudes 43.75° – 44.25°; 2) Central, latitudes 44.25° – 45.0°; and 3) Northern, latitude 45.0° – 45.75°.

In the Southern region (1), we note that residuals values trend towards 0 with an increase in frequency (i.e., with our model, higher frequencies are better modeled than lower frequencies in the South) for the Salem earthquake. In this region, there is also a

difference in residuals between earthquakes. In the Salem and Scotts Mills earthquakes, we notice that the residuals in this region are negative (our model predicts stronger shaking than is observed), except the southernmost station (ALVY, Figure 8). In contrast, the Springfield earthquake shows strong positive values here (observed shaking is higher than our model predicts).

In the Central region (2), we notice that with increasing frequency, residuals become more positive in the Salem earthquake, though not as significant as in the Southern region; there are no such frequency-dependent region-wide trends for the Scotts Mills and Springfield earthquakes here. There are small differences between earthquakes in this region, with widespread positive residuals in the Salem and Springfield earthquakes, and negative residuals to the west and positive residuals to the east in the Scotts Mills.

The Northern region (3) holds the largest number of recordings due to the heavily instrumented Portland region. For the Salem earthquake, this region has the best fit on average. For the Scotts Mills earthquake, this region shows strong positive residuals (i.e., our model is underpredicting shaking). The Springfield earthquake was recorded in only three stations in this region, located at the basin edge, meaning our results may be less indicative of clear basin amplification effects here.

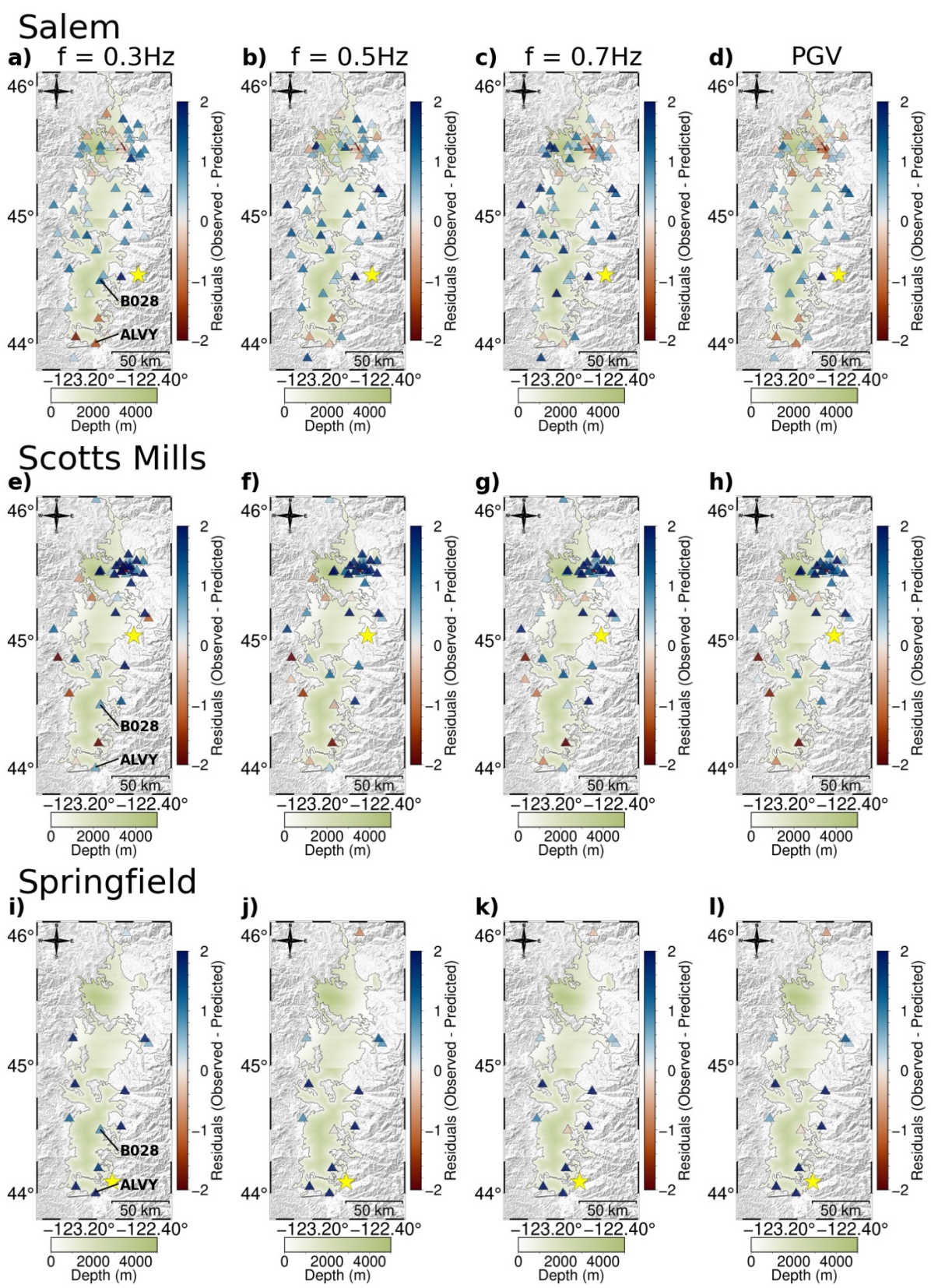
Salem
a) f = 0.3Hz
b) f = 0.5Hz
c) f = 0.7Hz
d) PGV
Scotts Mills
e)
f)
g)
h)
Springfield
i)
j)
k)
l)
B028
ALVY
50 km
−123.20°−122.40°
0 2000 4000
Depth (m)
Residuals (Observed - Predicted)
2
1
0
−1
−2
46°
45°
44°

Figure 6. Residuals maps for the Salem (top), Scotts Mills (middle) and Springfield (bottom) earthquakes (yellow stars), for f=0.3Hz, 0.5Hz, 0.7Hz, and PGV in the left, left-middle, right-middle, and right respectively. The maps are showing only Valley stations and are plotted on top of SRV 1D WV basin model (preferred model), colored by depth to bottom of the basin. Stations mentioned within the text are labeled.

Wave Propagation Snapshots

Snapshots of ground velocity (m/s) during specific time periods (t) of the wave propagation are useful in illuminating processes that contribute to the residual patterns that we see, and further our understanding of the performance of our model. We show a comparison of wave propagation snapshots, from two different time periods (t = 14 s and 25 s), and for each earthquake using our preferred model (SRV 1D) and the USGS CVM (Figure 7). The ground motion amplification of waves entering the WV is significantly stronger in our model than the USGS CVM. We observe a strong basin edge amplification that seemingly directs strong shaking into the WV basin. This amplification is absent in the USGS CVM simulations.

We note from these wave propagation snapshots that amplification in the WV appears to be the result of refraction and resonance of waves in the WV basin structure. The bottom panel of Figure 7 demonstrates this, showing that amplification of ground velocity at t=25s appears to be reduced from t=14s (when the waves enter the basin), though the ground velocity is still relatively strong and exists inside the borders of the basin. The simulations using the USGS CVM without WV characterization do not show the same strength of shaking at t=25s, and instead, we see that most of the energy has already dissipated within the WV.

We note several key propagation effects on shaking. Shaking in the Salem and Springfield earthquakes is amplified at basin edges more than in the Scotts Mills

earthquake (Figure 7a-f), implying an azimuthal source-path effect on shaking. This strong edge amplification in the Salem and Springfield events results in a longer duration of strong shaking within the basin, that maintains higher energy when traveling to the northern parts of the basin (Figure 7g,i,j,l; SVideo 01). In the Scotts Mill simulation, we see a divergence of the wavefield north of the epicenter, caused by the features in basin edge structure at this point in our model (Figures 7b,e,h,k). Such propagation effects may also contribute to the reduction in residuals seen at the North region of the model in the Scotts Mills earthquake (Figures 5, 6).

These plots also show how the added WV structure in our model impacts wave propagation, compared with the USGS CVM without WV sedimentary characterization. We see lower intensities produced in the USGS CVM compared to our model. At t=14s in the Salem and Springfield simulations, the SRV 1D model (Figure 7a and 7c), produces significantly stronger shaking when the waves are entering the valley compared to the same simulations using the USGS CVM (Figure 7d and 7f). At t=14s in the Scotts Mills simulations (Figure 7b and 7e), the differences between the SRV 1D model and the USGS CVM is less significant. We discuss these differences quantitatively later, when we examine seismic stations recordings' residuals, however, it seems related to the relatively detailed structure present in the northern region of the USGS CVM compared to the other regions of the WV (Stephenson et al., 2017), including a partial representation of the Portland and Tualatin basins.

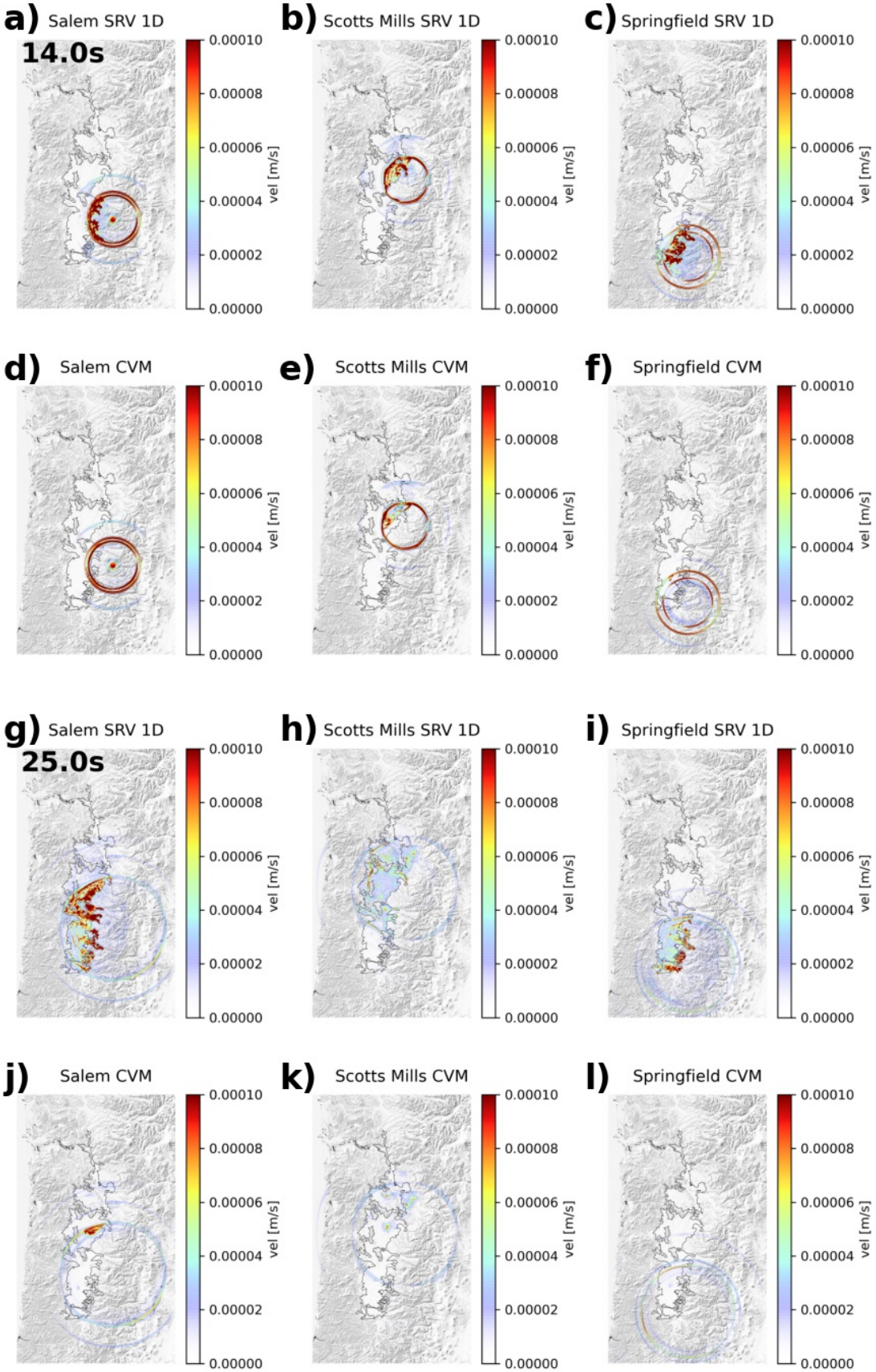
a) Salem SRV 1D
14.0s
b) Scotts Mills SRV 1D
c) Springfield SRV 1D
d) Salem CVM
e) Scotts Mills CVM
f) Springfield CVM
g) Salem SRV 1D
25.0s
h) Scotts Mills SRV 1D
i) Springfield SRV 1D
j) Salem CVM
k) Scotts Mills CVM
l) Springfield CVM
0.00010
0.00008
0.00006
0.00004
0.00002
0.00000
vel [m/s]

Figure 7. Maps of shaking intensity from wave propagation for the three earthquakes, showing snapshots of ground velocity. The top three maps, in each time (t) (a-b and g-i), are from simulations using the SRV 1D model and the bottom three maps (d-f and j-l) from simulations using the USGS CVM. Panels a-f show Vs magnitude after 14 seconds of the simulation (t=14s). Panels g-l how Vs magnitude after 25 seconds of the simulation (t=25s).

Waveform and Spectra Comparison

We present a handful of waveform and spectra comparisons, from seven stations located throughout the WV (Figure 8) to complement observations highlighted in the previous results sections.

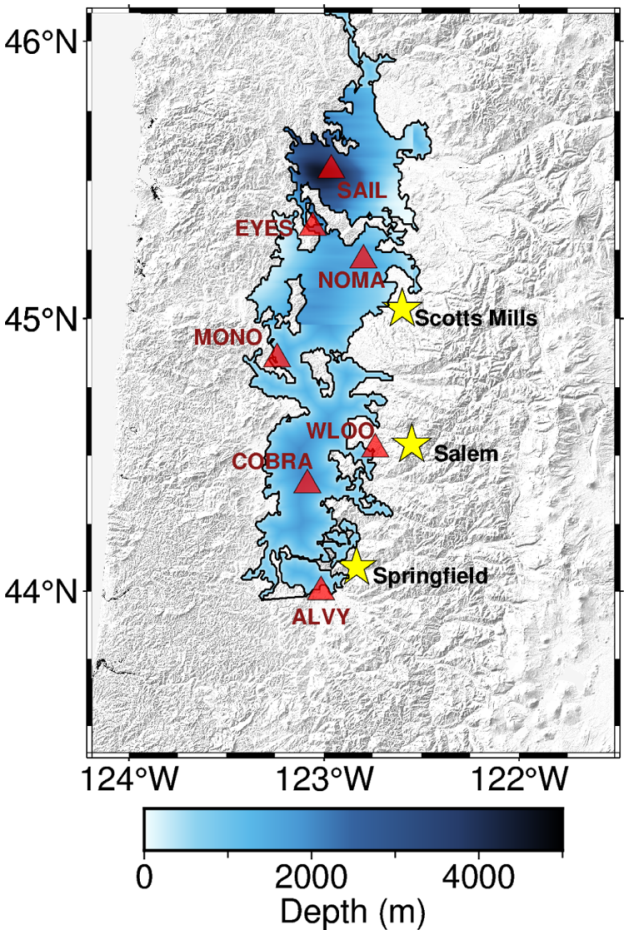

Figure 8. Basin map showing the location of stations for which waveforms and spectra are presented in this section. Red triangles are station locations; yellow stars are epicentral locations of the earthquakes recorded at these stations and shown in this section. Blue filling of the basin model represents the SRV 1D basin depth model.

MONO and ALVY (Figure 9) exemplify the significant inter-event variability we observe at some stations, and demonstrate how basin geometry may still be unconstrained in our model. MONO is located at the central western edge of the basin. In the Salem earthquake (Figure 9a), our SRV 1D model captures the amplification of the observed waveform throughout the duration of shaking and across much of the frequency range (δ_{PGV}=0.26, $\delta_{FAS\_0.5}$=0.07), compared to the USGS CVM (δ_{PGV}=1.44, $\delta_{FAS\_0.5}$=2.29). The exception is for two peaks in spectral amplitude in the observed data (~0.3Hz and ~0.9Hz), that are not captured in our model's spectrum. In the Scotts Mills earthquake (Figure 9c), the SRV 1D model fits the peak amplitude of the observed MONO waveform (δ_{PGV}=0.24) though not duration (i.e., after ~30s), but both the SRV 1D and USGS CVM spectra are lower in amplitude than the observed spectra ($\delta\{\text{SRV 1D}\}_{FAS\_0.6}$=0.51, $\delta\{\text{CVM}\}_{FAS\_0.6}$=1.24). In the Springfield earthquake (Figure 9e), the SRV_1D an USGS CVM spectra are also both lower in amplitude than the observed data, but significantly more than for the other two events ($\delta\{\text{SRV 1D}\}_{PGV}$=2.37, $\delta\{\text{CVM}\}_{PGV}$=2.36; $\delta\{\text{SRV 1D}\}_{FAS\_0.6}$=2.43, $\delta\{\text{CVM}\}_{FAS\_0.6}$=2.35). The amplification at ~0.3Hz, seen in the other earthquakes as well, is very strong in the observed data and absent from both synthetics, suggesting some unconstrained geology in our model.

ALVY is located at the southern edge of the model basin. In the Salem earthquake (Figure 9b), our model produces much higher PGV and spectral amplitudes than either the observed data, or the CVM (which underpredicts shaking here, $\delta\{\text{SRV 1D}\}_{PGV}$=-1.11, $\delta\{\text{CVM}\}_{PGV}$=0.36; $\delta\{\text{SRV 1D}\}_{FAS\_0.6}$=-0.73, $\delta\{\text{CVM}\}_{FAS\_0.6}$=1.33), although our model better predicts the duration of shaking. In Scotts Mills earthquake (Figure 9d), our model

and the USGS CVM both underestimate shaking, however our model better predicts the peak amplification ($\delta\{\text{SRV 1D}\}_{PGV}$=-0.06, $\delta\{\text{CVM}\}_{PGV}$=0.33), and better matches observed amplitudes at later times (>50s). The spectra show that our model captures a peak at ~0.7Hz that also exists in the observed ($\delta_{FAS\_0.6}$=0.23, $\delta_{FAS\_0.7}$=0.42). In contrast, the Springfield earthquake (Figure 9f) shows very similar properties as at MONO. The observed data is significantly stronger than both synthetics, with observed spectral peaks at ~0.3 and ~0.7Hz not or barely present in the synthetics ($\delta\{\text{SRV 1D}\}_{FAS\_0.3}$=2.42, $\delta\{\text{CVM}\}_{FAS\_0.3}$=2.38; $\delta\{\text{SRV 1D}\}_{FAS\_0.7}$=2.7, $\delta\{\text{CVM}\}_{FAS\_0.7}$=2.76).

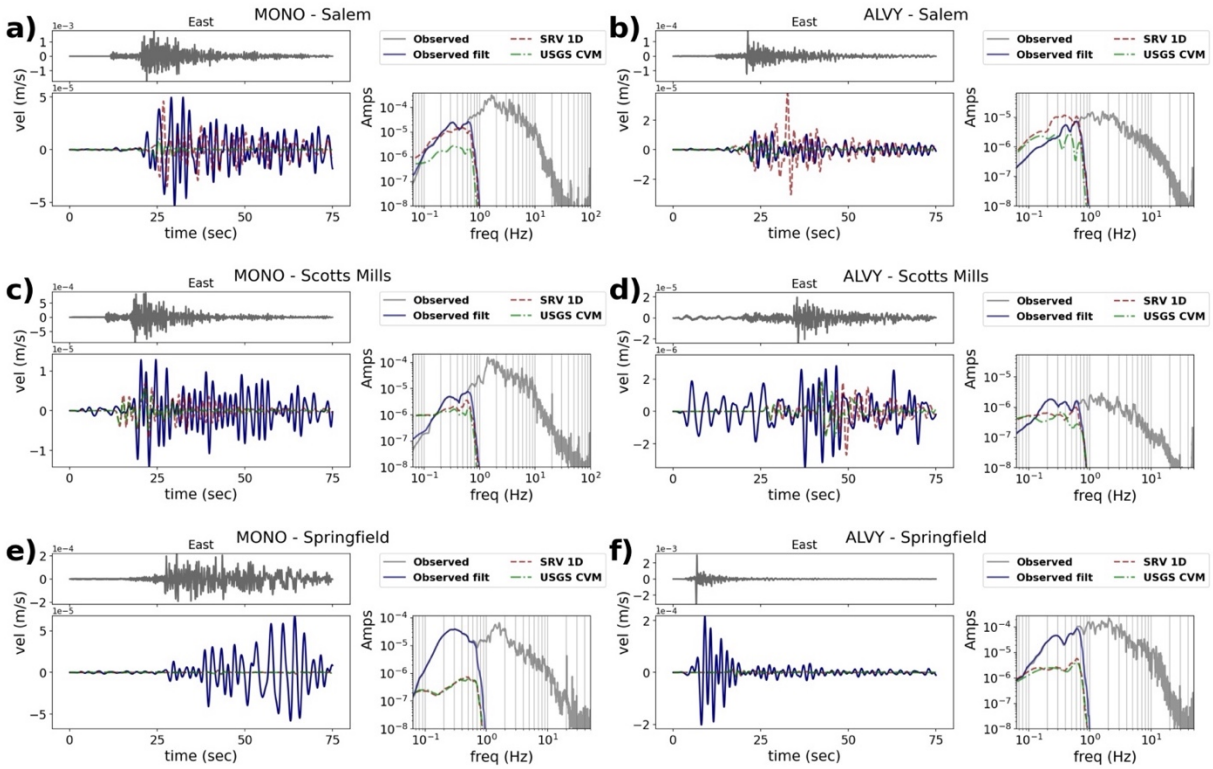

Figure 9. Waveform and spectra from the three earthquakes (Salem, Scotts Mills, Springfield) at two stations (MONO, ALVY), with each panel representing the observed and synthetic data recorded for that station-earthquake pair. Unfiltered waveforms are in grey, single waveform at the top left of each panel; the three filtered (max

frequency = 1Hz) waveforms are shown for the observed data (blue), SRV 1D model (red), and USGS CVM model (green). The spectra comparison are the same colors as the waveforms.

Stations WLOO and SAIL demonstrate misfits that may be indicative of inaccuracies in our definition of the WV basin's spatial extent definition (Figure 10). SAIL only records the Salem and Scotts Mills earthquakes, thus we compare only these events at both WLOO and SAIL. (Full data for all stations are in the supplemental material to this work).

WLOO is, in our model, a basin edge station. In the Salem earthquake (Figure 10a), there is very high observed amplitude peak in the waveform shortly after the S-wave arrival (~10s), and strong spectral peak at ~0.3Hz that are completely absent from both synthetics ($\delta\{\text{SRV 1D}\}_{\text{PGV}}$=3.96, $\delta\{\text{CVM}\}_{\text{PGV}}$=4.1, $\delta\{\text{SRV 1D}\}_{\text{FAS\_0.3}}$=4.45, $\delta\{\text{CVM}\}_{\text{FAS\_0.3}}$=4.57). There is also significant long-duration amplification observed in Scotts Mills earthquake (Figure 10c), not captured by our model or the USGS CVM, that could be attributed to a basin effect. The Scotts Mills simulations similarly do not match the observed peak or long-duration amplitudes observed ($\delta\{\text{SRV 1D}\}_{\text{PGV}}$=0.94, $\delta\{\text{CVM}\}_{\text{PGV}}$=0.93, $\delta\{\text{SRV 1D}\}_{\text{FAS\_0.3}}$=1.4, $\delta\{\text{CVM}\}_{\text{FAS\_0.3}}$=1.51). These observations may imply that the basin model should extend to include WLOO, to capture the observed amplification. We also note at WLOO the synthetics from our model and the CVM are nearly identical, likely because our model is identical to the USGS CVM outside our basin extent (see model construction section).

SAIL is located at the northern part of our model in the Tualatin basin, and may exemplify how the spatial extent of our basin model diffracts energy out of the basin (i.e., divergence of the wavefield, Figure 7b), generating a significant difference in residuals between the Salem and Scotts Mills earthquakes (Figures 5 and 6). In the Salem earthquake

(Figure 10b), our model is able to predict the peak shaking amplitude and spectra relatively well, while the USGS CVM produces significantly lower shaking than observed ($\delta\{\text{SRV 1D}\}_{\text{PGV}}$=0.25, $\delta\{\text{CVM}\}_{\text{PGV}}$=1.28; $\delta\{\text{SRV 1D}\}_{\text{FAS\_0.5}}$=0.005, $\delta\{\text{CVM}\}_{\text{FAS\_0.5}}$=1.57). Yet, our model does not capture amplification at longer durations (>~60s). In the Scotts Mills earthquake (Figure 10d), we see a significant amplification in the observations that is completely absent from both our model's and the CVM's spectra ($\delta\{\text{SRV 1D}\}_{\text{PGV}}$=2.84, $\delta\{\text{CVM}\}_{\text{PGV}}$=2.86, $\delta\{\text{SRV 1D}\}_{\text{FAS\_0.5}}$=2.68, $\delta\{\text{CVM}\}_{\text{FAS\_0.5}}$=2.79). This observation aligns with the high residuals we see near SAIL in this event, as the diverging wavefield (Figure 7XX) caused by the point of the basin extent likely reduces the amplitude of the synthetics as they enter the basin here.

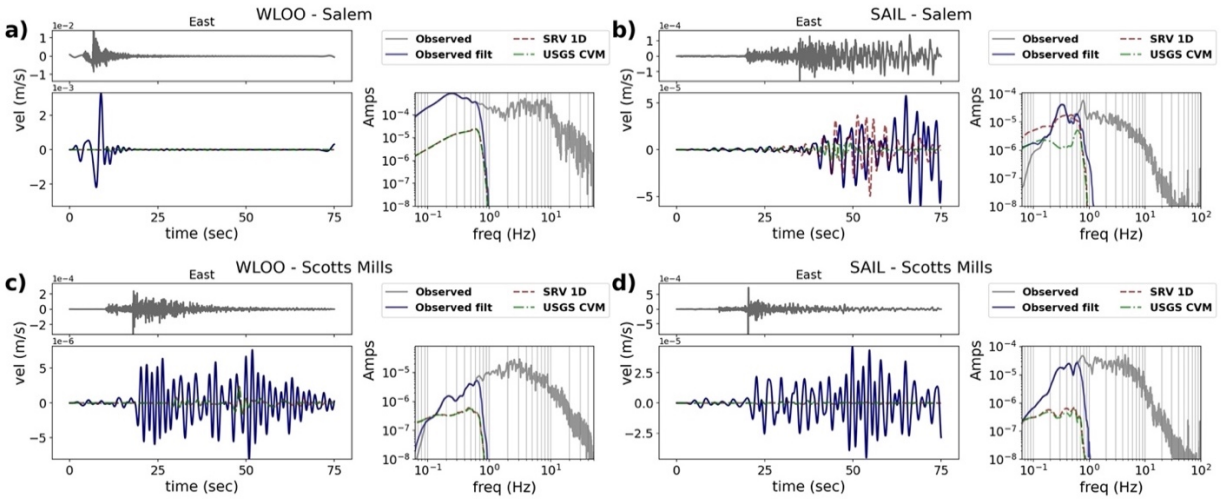

Figure 10. Waveform and spectra from the Salem and Scotts Mills earthquakes at two stations (WLOO, SAIL) with each panel representing the observed and synthetic data recorded for that station-earthquake pair. Unfiltered waveforms are in grey, single waveform at the top left of each panel; the three filtered (max frequency = 1Hz) waveforms are shown for the observed data (blue), SRV 1D model (red), and USGS CVM model (green). The spectra comparison are the same colors as the waveforms.

Lastly, we show data and synthetics from three stations inside the basin, to demonstrate the basin amplification our model is able to capture and the improvement it provides (Figure 11). COBRA is the only station located at the center of the Southern WV provides information on our model's performance here. Out of the three validation events we used, COBRA only recorded the Salem earthquake, thus we show only the data from the Salem earthquake for the two other stations (NOMA, EYES) as well.

At COBRA (Figure 11a), our model reproduces shaking intensity relatively well in the earlier stage of the waveform (~20 - ~40s, δ_{PGV}=0.76), however the observed waveform shows a strong second packet of energy, potentially a result of a basin amplification, that our model is not able to capture. The CVM is not able to capture the shaking intensity seen in the observed data, as it is significantly lower (δ_{PGV}=2.001). EYES (Figure 11b) is located at between the northern WV and Tualatin basin. Our model accurately captures the observed peak amplitude and long-duration shaking, though overpredicts intensities at ~35-50s (δ_{PGV}=-0.84). The CVM is neither able to produce the ringing, nor the shaking intensity of the observed. Our model's spectra more accurately captures the observed spectral peaks, which are absent from the USGS CVM's predictions ($\delta_{FAS\_0.3}$=-0.22, $\delta_{FAS\_0.7}$=-0.61; $\delta_{FAS\_0.3}$=1.34, $\delta_{FAS\_0.7}$=0.64).

NOMA (Figure 11c) is in northern WV and similar to the patterns highlighted in COBRA, the earlier part of the waveform (~25 - ~40s) fits the observed amplitude well (δ_{PGV}=0.65). In the later part of the waveform (>40s) our model produces stronger shaking than the observed data. In the synthetics, we do not see the clear second packet of energy at the later part of the earthquake, which is comparatively stronger in the observed at this station. This is, again, in contrast to the waveform the CVM produces, which is

significantly lower in amplitude and does not show any of the ringing seen in the observed data. Our model is also able to, partially, capture the peak spectral amplitude seen in the observed spectrum (~0.7Hz), though it is lower in amplitude ($\delta_{FAS\_0.7}$=0.14). The CVM seems to capture this peak as well, but in significantly lower amplitude than the observed ($\delta_{FAS\_0.7}$=1.35). Similar to COBRA and SAIL, both our model and the CVM produces higher spectral amplitudes in the lower frequencies (>0.1Hz).

Overall, these three stations exemplify the basin amplification that is present in the Willamette Valley, showing that our model, that includes a representation of the WV structure, performs much better than the USGS CVM, without the WV, at producing this amplification. At some stations (COBRA, NOMA) the amplification is not fully captured in our model, which may imply that the structure of our model, whether the velocity or the geometry) of the basin is not fully accurate.

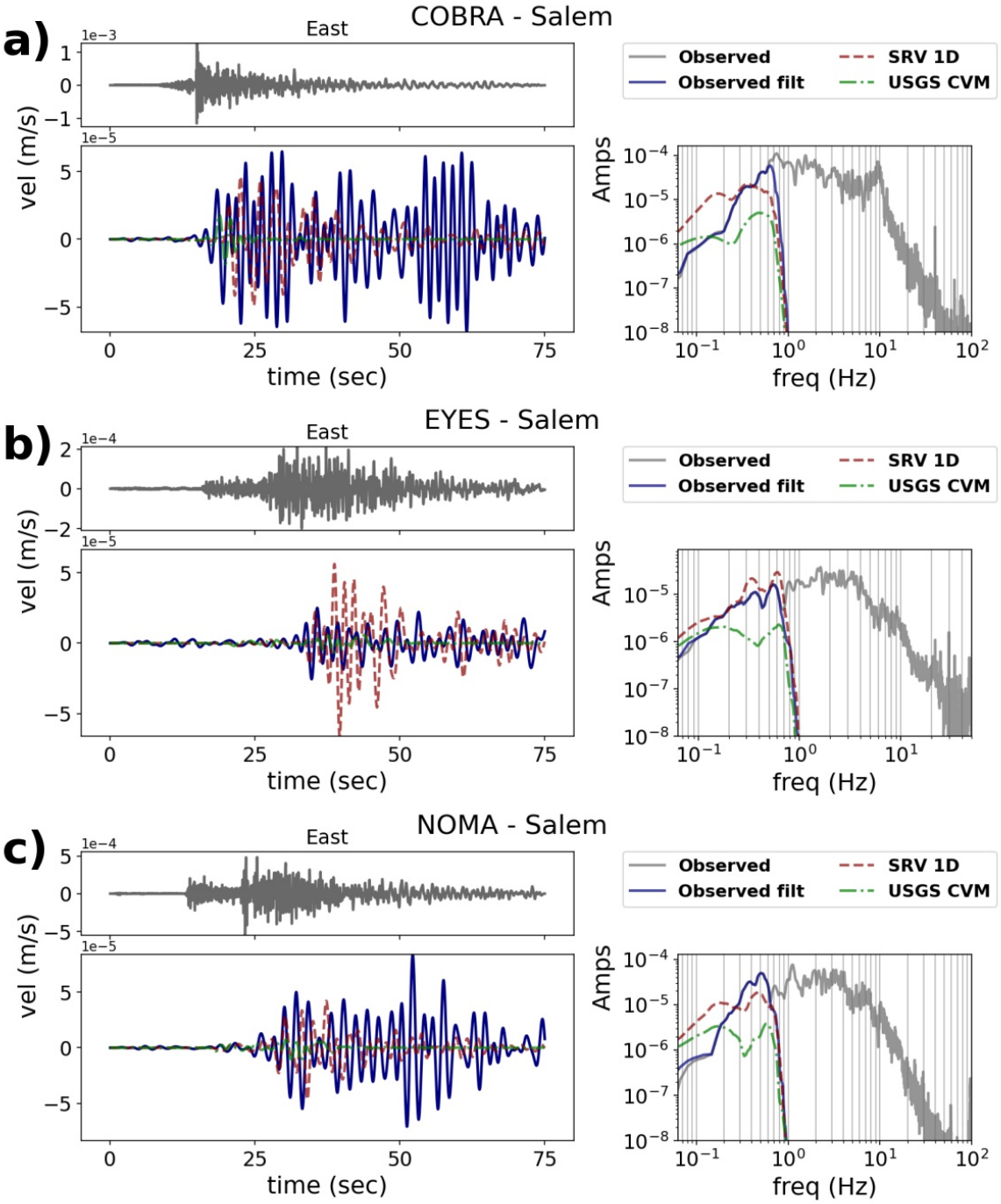

Figure 11. Waveform and spectra comparison from the Salem earthquake at three stations (COBRA, EYES, NOMA). Each panel shows the unfiltered waveform (grey, single waveform at the top left of each panel), a comparison of the three filtered (max frequency = 1Hz) waveforms (Blue – filtered observed, Red – SRV 1D model, Green – USGS CVM model) and a spectra comparison (same colors as waveforms).

Discussion

Performance Compared to the USGS CVM

The results we present show that our model performs better, on average, than the USGS CVM without WV characterization at replicating observed shaking intensities and duration in the valley stations throughout the WV. Since the difference between our model and the CVM is in the added structure of the WV basin, this suggests that a sedimentary "basin" structure exists in the WV and plays a significant role in controlling ground motions within it. This is highlighted in Figure 11, where we show how our model performs in the valley. The results from these stations show that our model captures the overall seismic amplification effects of the valley, though the accuracy of our model's predictions varies within the region, suggesting areas for future improvement. Here, we discuss these observations.

Inaccuracies of the Basin Model

We expect inaccuracies in our basin model due to the limited data available to constrain the valley's structure. Here, we identify three key features that could be improved upon. First, the geometry of the edges of the valley (spatial extent of the basin) are not well constrained. Our basin spatial extent was derived from the 400m/s contour of the USGS V_{S30} grid (Yong et al., 2016; Heath et al., 2020), thereby assuming that "soft" sediments as represented by V_{S30} values represented basin filling (i.e., hard rock valley edges would represent the extent of seismic basin effects), as they abut topographic contours and boundaries. This grid is mostly based on proxies such as topography, slope and lithology, and thus, reduces the accuracy of the V_{S30} values compared to measured values (Yong, 2016). Moreover, V_{S30} cannot fully predict where deep basin is located. A low V_{S30} value

does not necessarily mean that a deep basin lies beneath the measured point, as shown by relationships between V_{S30} and Z2.5 (Campbell & Bozorgnia, 2014). Other values, such as Z1.0 and Z2.5, that can serve as a more accurate proxies to estimate the spatial extent of the basin, are not available in this region as they are themselves dependent on characterization of deep sedimentary structures.

This inaccuracy is exemplified in comparing data and synthetics at WLOO (Figure 9). At this station, the synthetic data from our model (and from the CVM) show no basin effect on ground motions, while the observed data show a significant effect. This suggests that at this location, our basin should expand towards the east. An additional effect of simulation artifacts due to inaccurate valley edge definition is the diffraction in the wavefield during the Scotts Mills earthquake, caused by a sharp point in the valley outline. Close to the epicenter of the Scotts Mills earthquake, this point diffracts this earthquake's wavefield as it propagates northward (Figure 7). Its effect can be seen in SAIL station in Figure 9, where the Scotts Mills simulation significantly underpredict the observed, while the Salem simulation has a good overall fit.

Second, the geometry of the basement (i.e., basin depth geometry) is also not well constrained. Due to scarcity of input data, the geometry of the southern part of our model is based on a calibrated distance from the edge of every point within the valley. This results in a classic basin shape, that is deepest at its center and tapers out towards the edges but is not necessarily the actual shape of this basin. As they interact with seismic wavefields, the shape, width and depth of the basin can have a strong effect on the amplitude of shaking and the amplified frequencies that contribute to seismic basin effects (Cruz-Atienza et al., 2016; Sahakian et al., 2018). We hypothesize that the variability in our model's accuracy

at MONO and ALVY are demonstrative of this. The azimuthal direction and path length for recordings of all three earthquakes at these two stations varies and may suggest that a path effect is controlling the differences in fit we are seeing. This is important for not only improving future iterations of this model but also in consideration of nonergodic ground motion models (Landwehr et al., 2016; Sahakian et al., 2019; Sung & Abrahamson, 2022; Lavrentiadis et al., 2023). More specifically, MONO (Figure 10), located at the western edge of the valley, shows a relatively good fit for the Salem (δ_{PGV}=0.26, $\delta_{FAS\_0.5}$=0.07) and Scott Mills earthquakes (δ_{PGV}=0.24, $\delta_{FAS\_0.6}$=0.51), and a poor fit to Springfield (δ_{PGV}=2.37, $\delta_{FAS\_0.6}$=2.43). To reach this station, the wavefield must cross the valley, suggesting that the geometry of the basin and interaction with the wavefield likely affects amplification at this site.

Similarly, station ALVY (Figure 10) is very close to the epicenter of Springfield earthquake. At such short distances, it is possible that the arrivals are from predominantly vertically-traveling waves. Since the thickness of the basin in these locations are relatively low, the result is a very minimal interaction between the traveling waves and the relatively soft basin filling in our model, resulting in lower shaking amplitudes in these stations. It is important to note that the two examples given here show a significant underprediction for the Springfield earthquake. At first glance, this may suggest that the reported source magnitude which we use in our simulations is lower than it should be. However, we see several stations that show the exact opposite result, where the fit for the Springfield is better than the other two earthquakes and overpredicted at some stations as well (available to examination in supplementary material of this work), suggesting to us that our observations may represent path effects, or potentially a poorly constrained moment tensor.

Finally, due to the limited velocity profile data, it is likely that the shallow velocities in our model are not well constrained. For example, as mentioned above, our basin outlines are derived from the 400 m/s contour of the USGS V_{S30} grid. This means that the V_{S30} values inside the WV are, for the most part, lower than 400 m/s (and perhaps even lower than 100 m/s at specific locations, according to the USGS grid). Due to computational demands, the minimum Vs value in our model is 600 m/s. This creates a known inaccuracy that could be significant in capturing shaking amplitudes in the WV. The basin stations in our model do capture some of the basin amplification seen in the observed waveforms, but in many of them the shaking amplitude is not sufficiently amplified. Since shallow velocities can significantly affect the amplitude of shaking at the surface, this inaccuracy in the basin structure can possibly affect the misfit we are seeing in the basin stations.

Basin Amplification Factor

To demonstrate the impact our model may have on amplification, we calculate a Basin Amplification Factor (BAF) for the WV (Figure 12), using Z2.5 from our model (the depth to the 2.5 km/s contour). We calculate this in two ways: 1) Estimating BAF with shaking values using a ground motion model (GMM) with basin terms (specifically Z2.5) extracted from our model, and 2) using shaking values from our simulations' data. In both ways we estimate shaking as peak ground velocity (PGV) at each grid point within our model's domain. For (1), we compute the BAF as:

$$BAF = \frac{1}{n}\sum_{i=1}^{n}\frac{PGV^{i}_{GMM,Basin}}{PGV^{i}_{GMM,No\ Basin}} \quad (5)$$

where n is number of basin grid points the shaking ratio were calculated, $PGV^{i}_{GMM,Basin}$ is the shaking value estimated using the GMM with basin terms and $PGV^{i}_{GMM,No\ Basin}$ is the shaking value without a basin term. We estimate ground motions with the Parker 2020 NGA-Sub GMM, on the OpenQuake Engine platform (Parker et al., 2021; Pagani et al., 2024), which implements a regional Cascadia basin adjustment factor. NGA-Sub estimates basin amplification using Z2.5 (which we take as our Z2.5 grid, Figure 12a) and Vs30 (which we take from Heath et al., 2020, Figure 12b). The NGA-Sub basin amplification term is neither distance nor magnitude dependent, so we compute ground motions for all grid points assuming rupture (R_{RUP}) of 100km and **M**8 event, to represent a megathrust event along the CSZ. The regional amplification is shown in Figure 12c, and thus represents amplification from a potential megathrust (not crustal) event.

For the second method, we calculate the ratio between shaking values from our simulations using our basin model, and the simulations using the USGS CVM model as a reference. Here, we compute BAF, similarly to the first method, as:

$$BAF = \frac{1}{n}\sum_{i=1}^{n}\frac{PGV^{i}_{SRV\ 1D}}{PGV^{i}_{USGS\ CVM}} \quad (6)$$

For both methods, we present the average BAF for all grid points within the WV outline. We compute this for all three validation events in the study (Figure12d-f).

In the GMM shaking ratio map, we see a slightly higher BAF in the basin compared to its surroundings. However, we note that the V_{S30} values appear to have a stronger effect on estimated shaking than the Z2.5 values, and that the BAF value is relatively low compared to the BAF values calculated using the simulations data. This result may be due

to our near uniform basin filling (i.e., the velocity gradient is consistent everywhere in the basin and not grid-point dependent, Figure 3), resulting in nearly-uniform, relatively low Z2.5 values, may be accounted for by the relative amplification of VS30 compared to basin terms with our Z2.5 values, or may reflect the reliability of Z2.5 as a proxy in this region. In contrast, the simulation results show different spatial patterns of BAF for each of the simulated earthquakes. This corroborates with our previous results, suggesting a strong azimuthal dependency of shaking intensity, and likely path effects.

These results demonstrate that the basin structure presents an amplification effect, to be considered in future studies in this region. Z2.5 (and Z1.0) are obtainable with velocity models, but additional, simulation data such as what we present here are additionally a useful tool for estimating future amplification, as preferred in some studies over basin proxy terms (Z1.0 and Z2.5, Moschetti et al., 2024).

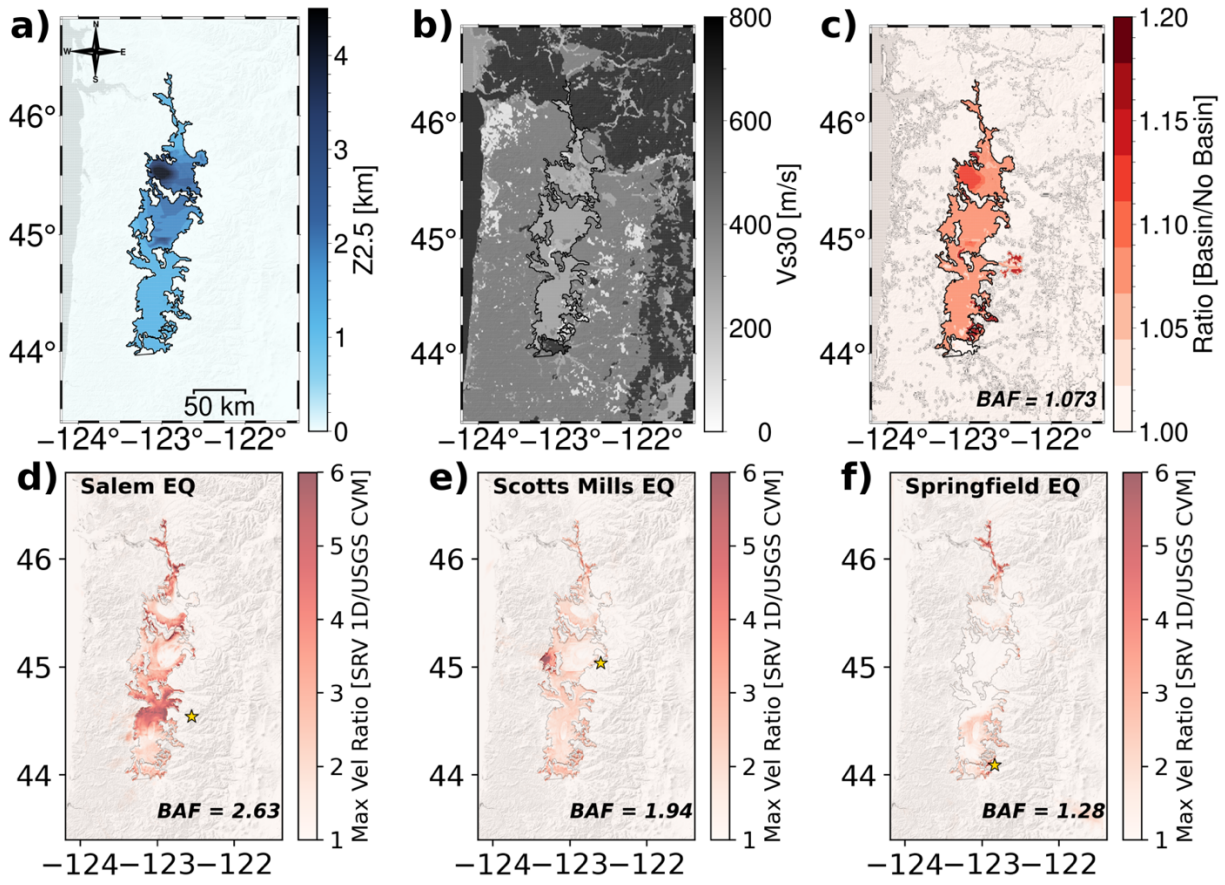

Figure 12. Basin Amplification Factor analysis summary. Top panels (a-c) show the data inputs, Z2.5 (a) and V_{S30} (b) used for the shaking calculations using OpenQuake Engine with the Parker et al. (2021) GMM, along with resulting shaking ratio map (c). Averaged BAF value is in bolded black text in the bottom right of 12c. Bottom panels (d-f) show maximum velocity ratio maps from the simulations of the Salem (d) Scotts Mills (e) and Springfield (f) earthquakes. Epicenters location are marked by a yellow star. Averaged BAF values are in bolded black text in the bottom right.

Areas for Further Improvement

Here, we highlight some areas that we believe could improve the accuracy of our model. One key feature of our model that we identify for improvement is the spatial extent (outline) of the basin. Since it is very hard to accurately determine basin boundaries without

an extensive subsurface dataset, which currently does not exist in this region, future iterations would benefit from a focus on updating the basin spatial extent based on the results we present here and by using similar methods with updated data. For example, since the development of our model, a new study on regional V_{S30} values (Geyin & Maurer, 2023) has been published and may also present updated V_{S30} contours that could be used as outlines.

A second recommendation is to explore the possibility of extended temporary broadband deployment or additional permanent instrumentation within the central and southern regions of the valley, to constrain both basement depth, impedance contrasts, and 1D velocity profiles of the sedimentary structures. Permanent seismic stations tend to be installed on hard rock to reduce noise, rather than softer material that the valley consists of, limiting our observational abilities in key portions of the valley that require site characterization. Potential methods to constrain basin depth and velocity profiles include HVSR (Molnar et al., 2018; Carpenter et al., 2023), krSPAC (Stephenson et al., 2019; Asten et al., 2023), site spectra from inversion methods (Klimasewski et al., 2019; Frankel & Grant, 2020), and other noise-based methods to characterize the subsurface velocities (Park & Ishii, 2018; Li & Park, 2024).

Finally, the dataset of constraints that could be used in model construction should be more comprehensive. New data from 1D profiles, gravity data, active source surveys etc., should be obtained and incorporated. A larger and updated dataset is crucial for the improvement of the accuracy of the model.

Conclusion

We constructed a new velocity model of the WV region, based on available geologic, geophysical and structural data. This model, using the Siletz River Volcanic formation as basement and a 1D velocity gradient from oil and gas well data (SRV 1D), was selected as our preferred model amongst three other models differing in structural characteristics (i.e., basin depth and sedimentary velocity structure). We tested these models against recorded data from three local crustal earthquakes, comparing synthetic data from numerical simulations with the observed waveforms. We calculated residual values between the synthetics and observations using several different intensity measures (PGV and FAS binned to 0.2, 0.3, 0.4, 0.5, 0.6, 0.7 Hz). Overall, our models perform better in fitting the observed data compared to the current regional velocity model (USGS CVM), which does not include the Willamette Valley. This implies that the sedimentary structure of the WV, which is mostly absent from the USGS CVM, has a significant effect on ground motions in this region.

However, our model is not able to fully capture the effect of the WV, and shows misfits in predicting the amplification seen in the observed data, likely due to inaccuracies in our model's structure. This is unsurprising, as we made some assumptions due to limited data available to constrain the structure. We note that that these inaccuracies can be focused to the spatial extent of our modeled "basin" and the geometry of the basin's depth. Future iterations of this model would benefit from focusing on improving these aspects of the model, using updated information, and collecting new subsurface data that will help to better constrain this structure.

Our findings have important implications on seismic hazard assessment in this region. They help to refine our understanding of the effect that WV structure has on amplifying regional ground motions, which in turn, contributes to more accurate seismic hazard assessment.

Acknowledgements

This work was funded partially on grants EHP award G23AP00048-00 and NASA ROSES grant 80NSSC21K0841. We would like to acknowledge Ray Wells for helpful discussions regarding regional geology; William Stephenson for discussions of methods and likely structure in the region, as well as results; and R.S. degree committee members E. Hooft, J. Dufek, and D. Melgar for work and manuscript suggestions.

Data and Code Availability Statement

All data used in this study (digitized oil and gas well logs, input data, basin models, post-processed waveforms, simulation input files, simulation output, residuals flatfiles, Z1.0 and Z2.5 basin maps) can be found on Zenodo: https://zenodo.org/records/13830998?preview=1&token=eyJhbGciOiJIUzUxMiJ9.eyJpZCI6IjEwNDNkMzRkLTU5MzItNDRjZC05Y2ZiLTBhNWYxMmRjZjhhOSIsImRhdGEiOnt9LCJyYW5kb20iOiJkMzM3MzA5OTcwNWZlZGUyZThkZDk0NjZhMTcxNmYxZiJ9.Un2ad5LFwW37MgHfl2lq6Wk48z_f-c_FRCvSBHzk078U0pqgQyWJyvu-tT9_4ULt4AgaJ2FeBgfGFUM-fmb4Lw.

All code from this study can be found at https://github.com/rshimony.

References

Atwater, B. F., & Hemphill-Haley, E. (1997). Recurrence Intervals for Great Earthquakes of the Past 3,500 Years at Northeastern Willapa Bay, Washington. *United States Geological Survey Professional Paper*, *P 1576*, 108 pp.

Baltay, A. S., & Boatwright, J. (2015). Ground-motion observations of the 2014 South Napa Earthquake. *Seismological Research Letters*, *86*(2A), 355–360. https://doi.org/10.1785/0220140232

Bassett, D., & Watts, A. B. (2015). Gravity anomalies, crustal structure, and seismicity at subduction zones: 2. Interrelationships between fore-arc structure and seismogenic behavior. *Geochemistry, Geophysics, Geosystems*, *16*(5), 1541–1576. https://doi.org/10.1002/2014GC005685

Bayless, J., & Abrahamson, N. A. (2018). Evaluation of the interperiod correlation of ground-motion simulations. *Bulletin of the Seismological Society of America*, *108*(6), 3413–3430. https://doi.org/10.1785/0120180095

Blakely, R. J., Wells, R. E., Tolan, T. L., Beeson, M. H., Trehu, A. M., & Liberty, L. M. (2000). New aeromagnetic data reveal large strike-slip (?) faults inthe Northern Willamette Valley, Oregon. *Bulletin of the Geological Society of America*, *112*(8), 1225–1233. https://doi.org/10.1130/0016-7606(2000)112<1225:NADRLS>2.0.CO;2

Borcherdt, R. D., & Gibbs, J. F. (1976). *Effects of local geological conditions in the San Francisco bay region on ground motions and the intensities of the 1906 earthquake*. *Bull. Seism. Soc. Am.* (Vol. 66).

Brocher, T. M. (2008). Key elements of regional seismic velocity models for long period ground motion simulations. *Journal of Seismology*, *12*(2), 217–221. https://doi.org/10.1007/s10950-

007-9061-3

Campillo, M., Gariel, J. C., Aki, K., & Sanchez-Sesma, F. J. (1989). Destructive strong ground motion in Mexico City: source, path, and site effects during great 1985 Michoacan earthquake. *Bulletin - Seismological Society of America*, *79*(6), 1718–1735. https://doi.org/10.1785/bssa0790061718

Cruz-Atienza, V. M., Tago, J., Sanabria-Gómez, J. D., Chaljub, E., Etienne, V., Virieux, J., & Quintanar, L. (2016). Long Duration of Ground Motion in the Paradigmatic Valley of Mexico. *Scientific Reports*, *6*(November), 1–9. https://doi.org/10.1038/srep38807

Eberhart-Phillips, D., Thurber, C., & Fletcher, J. B. (2014). Imaging P and S attenuation in the Sacramento–San Joaquin Delta Region, Northern California. *Bulletin of the Seismological Society of America*, *104*(5), 2322–2336. https://doi.org/10.1785/0120130336

Frankel, A., & Grant, A. (2021). Site response, basin amplification, and earthquake stress drops in the Portland, Oregon area. *Bulletin of the Seismological Society of America*, *111*(2), 671–685. https://doi.org/10.1785/0120200269

Frankel, A., Wirth, E., Marafi, N., Vidale, J., & Stephenson, W. (2018). Broadband synthetic seismograms for magnitude 9 earthquakes on the cascadia megathrust based on 3D simulations and stochastic synthetics, Part 1: Methodology and overall results. *Bulletin of the Seismological Society of America*, *108*(5), 2347–2369. https://doi.org/10.1785/0120180034

Geyin, M., & Maurer, B. W. (2023). U.S. National VS30 Models and Maps Informed by Remote Sensing and Machine Learning. *Seismological Research Letters*, *94*(3), 1467–1477. https://doi.org/10.1785/0220220181

Heath, D. C., Wald, D. J., Worden, C. B., Thompson, E. M., & Smoczyk, G. M. (2020). A global

hybrid VS30 map with a topographic slope–based default and regional map insets. *Earthquake Spectra*, *36*(3), 1570–1584. https://doi.org/10.1177/8755293020911137

Kawase, H. (1996). The cause of the damage belt in Kobe: "The basin-edge effect," constructive interference of the direct S-wave with the basin-induced diffracted/Rayleigh waves. *Seismological Research Letters*, *67*(5), 25–34. https://doi.org/10.1785/gssrl.67.5.25

McNeill, L. C., Goldfinger, C., Kulm, L. V.D., & Yeats, R. S. (2000). Tectonics of the Neogene Cascadia forearc basin: Investigations of a deformed late Miocene unconformity. *Bulletin of the Geological Society of America*, *112*(8), 1209–1224. https://doi.org/10.1130/0016-7606(2000)112<1209:TOTNCF>2.0.CO;2

McPhee, D. K., Langenheim, V. E., Wells, R. E., & Blakely, R. J. (2014). Tectonic evolution of the tualatin basin, northwest Oregon, as revealed by inversion of gravity data. *Geosphere*, *10*(2), 264–275. https://doi.org/10.1130/GES00929.1

Nye, T., Sahakian, V. J., King, E., Baltay, A., & Klimasewski, A. (2023). Estimates of κ0 and Effects on Ground Motions in the San Francisco Bay Area. *Bulletin of the Seismological Society of America*, *113*(2), 823–842. https://doi.org/10.1785/0120220046

Obermeier, S. F., & Dickenson, S. E. (2000). Liquefaction evidence for the strength of ground motions resulting from Late Holocene Cascadia subduction earthquakes, with emphasis on the event of 1700 A.D. *Bulletin of the Seismological Society of America*, *90*(4), 876–896. https://doi.org/10.1785/0119980179

Petersen, M. D., Shumway, A. M., Powers, P. M., Mueller, C. S., Moschetti, M. P., Frankel, A. D., et al. (2020). The 2018 update of the US National Seismic Hazard Model: Overview of model and implications. *Earthquake Spectra*, *36*(1), 5–41. https://doi.org/10.1177/8755293019878199

Petersen, M. D., Shumway, A. M., Powers, P. M., Field, E. H., Moschetti, M. P., Jaiswal, K. S., et al. (2024). *The 2023 US 50-State National Seismic Hazard Model: Overview and implications*. *Earthquake Spectra* (Vol. 40). https://doi.org/10.1177/87552930231215428

Petersson, N. A., & Sjögreen, B. (2015). Wave propagation in anisotropic elastic materials and curvilinear coordinates using a summation-by-parts finite difference method. *Journal of Computational Physics*, *299*, 820–841. https://doi.org/10.1016/j.jcp.2015.07.023

Petersson, N. A., & Sjögreen, B. (2017). User's guide to SW4, version 2.0. *Lawrence Livermore National Laboratory Tech. Rept. LLNL-SM*, *741439*.

Silva, W., Wong, I., Darragh, R., & Rogers, A. (1998). Engineering characterization of earthquake strong ground motions in the Pacific Northwest. *Assessing Earthquake Hazards and Reducing Risk in the Pacific Northwest 1560*, *1560*, 313–324.

Sjögreen, B., & Petersson, N. A. (2012). A fourth order accurate finite difference scheme for the elastic wave equation in second order formulation. *Journal of Scientific Computing*, *52*(1), 17–48. https://doi.org/10.1007/s10915-011-9531-1

Stephenson, W. J., Reitman, N. G., & Angster, S. J. (2017). P- and S-wave velocity models incorporating the Cascadia subduction zone for 3D earthquake ground motion simulations, version 1.6 — Update for Open-File Report 2007–1348. *U.S. Geological Survey Open-File Report 2017–1152*, (September), 17. https://doi.org/10.3133/ofr20171152

Thompson, M., Wirth, E. A., Frankel, A. D., Hartog, J. R., & Vidale, J. E. (2020). Basin amplification effects in the Puget Lowland, Washington, from strong-motion recordings and 3D simulations. *Bulletin of the Seismological Society of America*, *110*(2), 534–555. https://doi.org/10.1785/0120190211

Wald, D. J., & Graves, R. W. (1998). The seismic response of the Los Angeles basin, California.

Bulletin of the Seismological Society of America, *88*(2), 337–356.

Wang, Y., Lin, F. C., & Ward, K. M. (2019). Ambient noise tomography across the Cascadia subduction zone using dense linear seismic arrays and double beamforming. *Geophysical Journal International*, *217*(3), 1668–1680. https://doi.org/10.1093/gji/ggz109

Ward, K. M., Lin, F., & Schmandt, B. (2018). High-Resolution Receiver Function Imaging Across the Cascadia Subduction Zone Using a Dense Nodal Array. *Geophysical Research Letters*, *45*(22), 12,218-12,225. https://doi.org/10.1029/2018GL079903

Wells, R., Bukry, D., Friedman, R., Pyle, D., Duncan, R., Haeussler, P., & Wooden, J. (2014). Geologic history of Siletzia, a large igneous province in the Oregon and Washington Coast Range: Correlation to the geomagnetic polarity time scale and implications for a long-lived Yellowstone hotspot. *Geosphere*, *10*(4), 692–719. https://doi.org/10.1130/GES01018.1

Wells, R. E. (1998). Fore-arc migration in Cascadia and its neotectonic significance. *Geology*, *26*(8), 759–762. https://doi.org/10.1130/0091-7613(1998)026<0759:FAMICA>2.3.CO;2

Wirth, E. A., Frankel, A. D., Marafi, N., Vidale, J. E., & Stephenson, W. J. (2018). Broadband synthetic seismograms for magnitude 9 earthquakes on the cascadia megathrust based on 3D simulations and stochastic synthetics, Part 2: Rupture parameters and variability. *Bulletin of the Seismological Society of America*, *108*(5), 2370–2388. https://doi.org/10.1785/0120180029

Wirth, E. A., Vidale, J. E., Frankel, A. D., Pratt, T. L., Marafi, N. A., Thompson, M., & Stephenson, W. J. (2019). Source-Dependent Amplification of Earthquake Ground Motions in Deep Sedimentary Basins. *Geophysical Research Letters*, *46*(12), 6443–6450. https://doi.org/10.1029/2019GL082474

Yeats, R. S., Graven, E. P., Werner, K. S., Goldfinger, C., & Popowski, T. A. (1996). Tectonics

of the Willamette Valley, Oregon. US Geological Survey Professional Paper 1560.

Yong, A., Thompson, E. M., Wald, D. J., Knudsen, K. L., Odum, J. K., William J Stephenson, & Haefner, S. (2016). Compilation of Vs30 Data for the United States, 8 p.

Zhang, L., Wang, S., & Petersson, N. A. (2021). Elastic Wave Propagation in Curvilinear Coordinates with Mesh Refinement Interfaces by a Fourth Order Finite Difference Method. *SIAM Journal on Scientific Computing*, *43*(2), A1472–A1496. https://doi.org/10.1137/20M1339702